Research on photodiode integrated with wide spectrum focusing reflector using nonperiodic subwavelength gratings

Tao Liu (刘 涛), Yongqing Huang (黄永清)*, Jiarui Fei (费嘉瑞), Gang Wu (武 刚), Xiaokai Ma (马晓凯), Xiaofeng Duan (段晓峰), Kai Liu (刘 凯), and Xiaomin Ren (任晓敏)

Institute of Information Photonics and Optical Communications, Beijing University of Posts and Telecommunications, Beijing 100876, China

**Corresponding author: yqhuang@bupt.edu.cn*

Received December 18, 2017; accepted March 16, 2018; posted online April 27, 2018

The fabrication and characterization of p-i-n photodiodes integrated with wide spectrum focusing reflectors using nonperiodic strip and concentric-circular subwavelength gratings are presented. The experimental results show that the gratings can reflect and focus the incident light on the absorber of the photodiode, and thus can simultaneously achieve high speed and high efficiency. For the gratings' integrated photodiodes, the responsivity is improved over a wide spectral range, and when the absorber was 600 nm and the mesa diameter was 40 μm, a responsivity of 0.46 A/W at a wavelength of 1.55 μm and a 3 dB bandwidth of 21.6 GHz under a reverse bias of 3 V were simultaneously obtained.

OCIS codes: 130.3120, 230.5170, 250.0040.

doi: 10.3788/COL201816.051301.

Highspeed and high-efficiency p-i-n photodiodes (PDs) are critical components for optical communication systems. Typically, there is a trade-off between bandwidth and quantum efficiency for a p-i-n PD. The two major speed-limiting factors in p-i-n photodiodes that cause the trade-off are the transit time and resistor-capacitor (RC) time. The RC time limit can be alleviated either by employing a smaller device area or by increasing the depletion width, thereby decreasing the capacitance per unit area. However, an increased depletion width consequently increases the transit time. On the other hand, a smaller device area and a thinner absorption layer will reduce the efficiency of p-i-n PDs. To overcome this limitation, the traditional structure of resonant cavity enhanced p-i-n PDs[1–4] has been proposed. This structure can achieve a high speed, a high efficiency, and a narrow spectral linewidth. In addition, a PD integrated with a single bottom reflector such as a distributed Bragg reflector[5,6], periodic subwavelength gratings[7], or metal mirror[8] can obtain a high speed and high efficiency simultaneously because the effective absorption length of the devices has doubled.

It is worth noting that the spot size becomes larger due to scattering when the beam passes through the PD. Therefore, a PD integrated with a focusing reflector means that the coupling efficiency between the optical fiber and the PD can be improved compared with the normal reflector integrated PD. It is known to all that conventional focusing reflectors require an aspheric shape and bulky thickness, presenting difficulties for standard microfabrication techniques. Subwavelength gratings as reflectors are easy monolithically fabricated with other optoelectronic devices[9–11]. In addition, subwavelength gratings as broadband high-reflectivity reflectors with focusing abilities have been reported, such as nonperiodic strip subwavelength gratings (S-SWGs)[12] and nonperiodic concentric circular subwavelength gratings (CC-SWGs)[13–15]. In this Letter, we present the S-SWGs and CC-SWGs integrated with p-i-n PDs to simultaneously achieve a high speed and high efficiency.

The cross-sectional view of the p-i-n PD integrated with nonperiodic subwavelength gratings is shown in Fig. 1. It can be seen from the figure that the p-i-n PD has a 600 nm $In_{0.53}Ga_{0.47}As$ absorption layer, a 300 nm heavily doped p-type $In_{0.52}Al_{0.48}As$ electron barrier, a 100 nm heavily doped $In_{0.53}Ga_{0.47}As$ p-contact layer, a 600 nm heavily doped InP n-contact layer, and a 350 μm InP substrate. The metal electrodes are deposited on heavily doped p- and n-contact layers to form a good ohmic contact. The gratings consist of a 500 nm silicon bar layer, a 500 nm buried oxide layer, and a silicon substrate, which

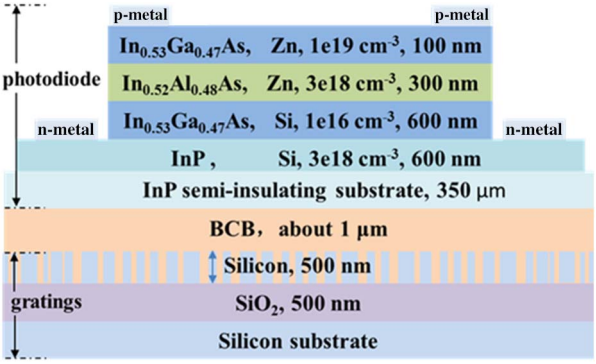

Fig. 1. Cross-sectional view of a p-i-n photodiode integrated with nonperiodic subwavelength gratings.

 © 2018 Chinese Optics Letters

is integrated at the bottom of the PD by a 1 μm benzocyclobutene (BCB) layer.

The S-SWGs and CC-SWGs with a focal length of 350 μm were fabricated on a silicon on insulator (SOI) wafer with the fabrication process as in Refs. [12–14]. The total structures of S-SWGs and CC-SWGs are a square of 500 μm × 500 μm and a circle with a 500 μm diameter, respectively. The optical microscope pictures of the fabricated S-SWGs and CC-SWGs and the groove width at various locations are shown in Fig. 2.

The performance of the fabricated SOI-based S-SWGs and CC-SWGs was measured before integration with p-i-n PDs. Figure 3 shows the power distribution at the reflection focal plane of the gratings. The incident light, with a wavelength of 1.55 μm and a power of 3.56 mW, was TM-polarized and coupled with a single mode fiber. For the S-SWGs and the CC-SWGs, the full width at half-maximum (FWHM) of the power distributions at the reflection focal plane is about 168 μm and 140 μm, respectively; the peak powers are approximately 414 μW and 463.5 μW, respectively; and the reflectivities calculated by integration are 80.4% and 84.59%, respectively. Clearly, the performance of the CC-SWGs is better than that of the S-SWGs. The reason for the larger tested FWHM may be due to proximity effects in the electron-beam lithography step as well as the surface roughness of the silicon grooves[15]. The tested FWHM of the power distribution at the reflection focal plane could be achieved much closer to the designed FWHM by improving the fabrication process[16,17].

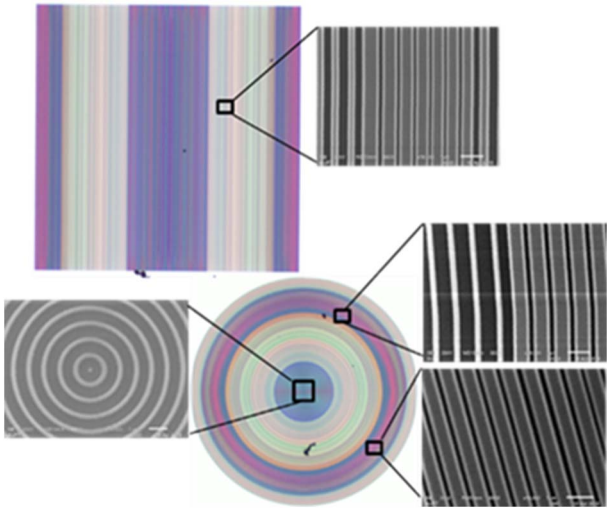

Fig. 2. Optical microscope pictures of the fabricated nonperiodic S-SWGs and nonperiodic CC-SWGs. The groove width at various locations is shown in scanning electron microscope (SEM) images in the insets.

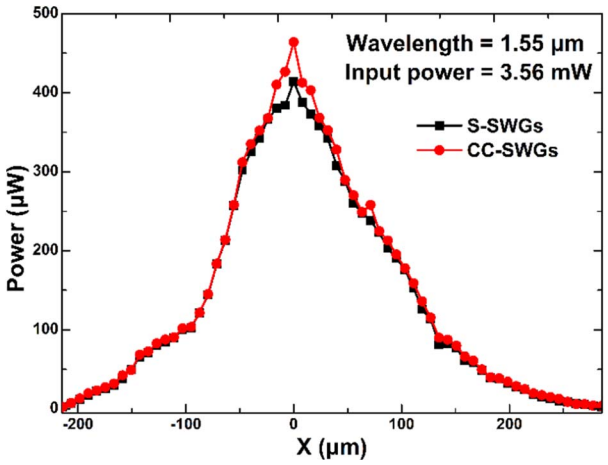

Fig. 3. Power distribution at the reflection focal plane of the fabricated gratings when the TM-polarized wave is incident.

The $In_{0.53}Ga_{0.47}As$/InP p-i-n PDs were fabricated by standard optoelectronic device processing steps including lithography, wet etching, p- and n-contact metallization, planarization, passivation, via hole opening, and pad metallization[18]. The PDs with mesa diameters of 40, 50, 80, 120, and 180 μm were prepared. The InP substrate of the PD was polished before integration. About a 1 μm thick BCB layer was used for the bonding of the PDs on the SOI-based gratings. The center of the PD mesa was aligned in the center of S-SWGs or CC-SWGs, and then the BCB was cured at 250°C for 2 h.

Figure 4 shows the relationship between the input power and the photocurrent, and the slope represents the responsivity. The DC measurements are carried out using a single mode fiber with an oblique head. It can be seen from the figure that the responsivity of the original PD is 0.38 A/W, and the responsivities of the PDs integrated with S-SWGs and CC-SWGs are increased to 0.481 A/W and 0.491 A/W, respectively. The responsivity of the CC-SWG-integrated PD is greater than that of the S-SWG-integrated PD because the performance of CC-SWGs is better than that of S-SWGs. In addition, a p-i-n PD integrated with the focusing reflector is first saturated with the increase of the input power due to its increased external quantum efficiency. The formula of external quantum efficiency (η) for the reflector-integrated PD is

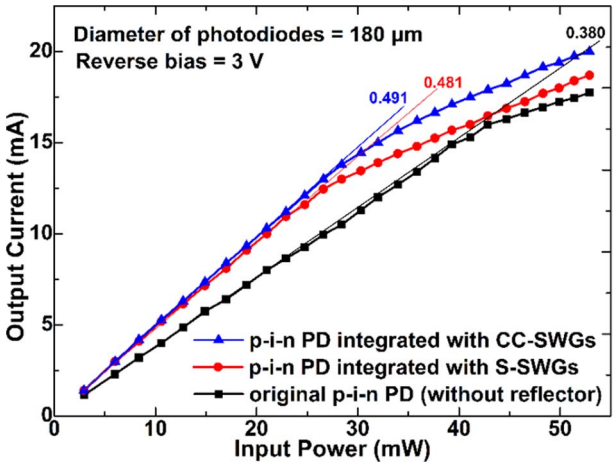

Fig. 4. Relationship between the input power and the output photocurrent.

$$\eta = (1 - r_1)e^{-\alpha d_1}(1 - e^{-\alpha d_2})(1 + re^{-\alpha d_2})f, \quad (1)$$

where r_1 is the reflectivity of the device surface, α is the absorption coefficient and is 0.65 μm^{-1} for $In_{0.53}Ga_{0.47}As$ at the wavelength of 1.55 μm, d_1 is the thickness of the $In_{0.53}Ga_{0.47}As$ contact layer, f represents the factors of electrical loss and other light loss, d_2 is the thickness of the active layer, and r is the reflectivity of the reflector. The external quantum efficiency (η) and responsivity (R) have the relation

$$R = \eta \frac{q\lambda}{hc}, \quad (2)$$

where q is the elemental charge, λ is the wavelength of the incident light, h is Planck's constant, and c is the speed of light. Substituting η from Eq. (1) into Eq. (2), we get the following expressions for the responsivity of the reflector-integrated PD:

$$R = R_0(1 + re^{-\alpha d_2}), \quad (3)$$

$$R_0 = (1 - r_1)e^{-\alpha d_1} f(1 - e^{-\alpha d_2}) \frac{e\lambda}{hc}. \quad (4)$$

It is worth noting that R_0 is 0.38 A/W according to the experimental results. Therefore, the reflectivity of the reflector can be calculated as follows:

$$r = (R/R_0 - 1)/e^{-\alpha d_2}. \quad (5)$$

The reflectivity of S-SWGs and CC-SWGs is 39.2% and 43.1%, respectively, according to the experimental results and Eq. (5). The reflectivity calculated in this way essentially eliminates the influence of the PD performance. The reason for the low reflectivity is that the reflectivity of the gratings is affected by the difference in the refractive index between silicon and the cladding layer[12–13]. The cladding layer before and after the integration is air and BCB. Therefore, we will consider using BCB as the cladding layer to design the gratings for the integration.

The measured response spectrum of different devices is displayed in Fig. 5 at the reverse bias of 3 V and the input power of 1.46 mW. Clearly, the responsivity of the photodiodes is improved in a wide spectral range after integration with the gratings. It can be deduced from the figure that the responsivity of the PDs tends to decrease as the wavelength of the incident light increases because the absorption coefficient of $In_{0.53}Ga_{0.47}As$ decreases as the wavelength increases from 1460 nm to 1610 nm. The responsivity of the original PD decreases with the increase of the mesa diameter. This indicates that the external quantum efficiency of the device decreases with the mesa area. It is worth noting that as the mesa diameter of the PDs decreases an increased responsivity difference between the grating-integrated PD and the original PD was observed under the same conditions. The responsivity of the grating-integrated PDs was almost unchanged at the wavelength of 1.55 μm as the mesa diameter decreases.

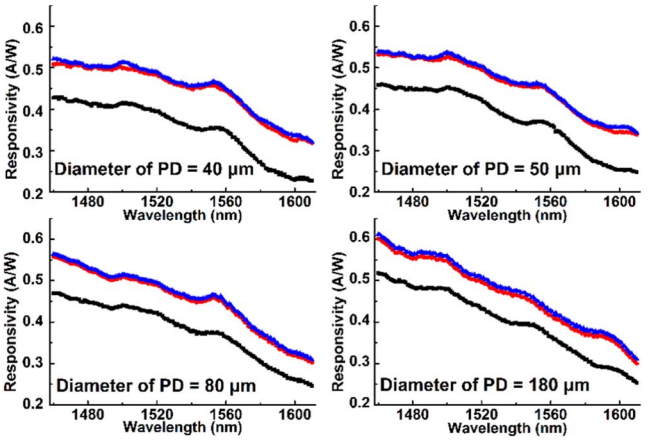

Fig. 5. Measured response spectra of different devices, when the reverse bias is 3 V and the input power is 1.46 mW. The black lines correspond to the original PD that is not integrated with a reflector. The red curves and the blue curves represent the PD integrated with S-SWGs and CC-SWGs, respectively.

Obviously, the main reason leading to the above two trends is that the gratings have focusing abilities. In addition, the 3 dB bandwidth of the PDs with mesa diameters of 40 μm and 50 μm is 21.6 GHz and 14.2 GHz, respectively, as shown in Fig. 6. This means the bandwidth of the PD can be improved by reducing the mesa area. Therefore, it is reasonable to believe that by increasing the reflectivity of the prepared gratings, especially by decreasing the FWHM of the focus to tens of micrometers, the bandwidth of the grating-integrated PDs can be improved by reducing the mesa diameter without the expense of external quantum efficiency. Consequently, the p-i-n PD with a relatively smaller mesa diameter and a thinner absorption layer integrated with the gratings can simultaneously achieve a high speed and high efficiency.

Figure 7 shows the efficiency-bandwidth product dependence on the input power for the PDs with mesa diameter of 50 μm. It can be seen from the figure that

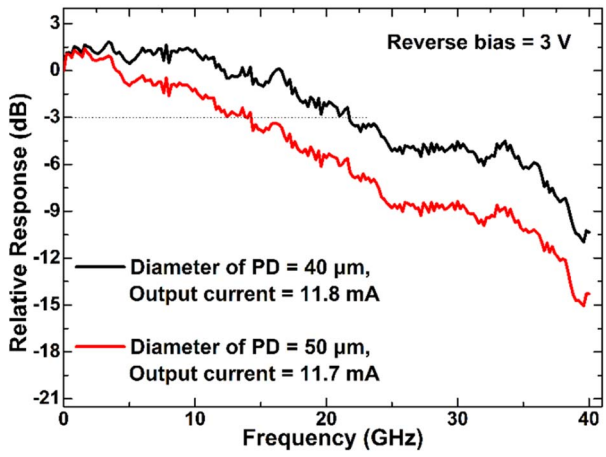

Fig. 6. Relative frequency response of the PDs.

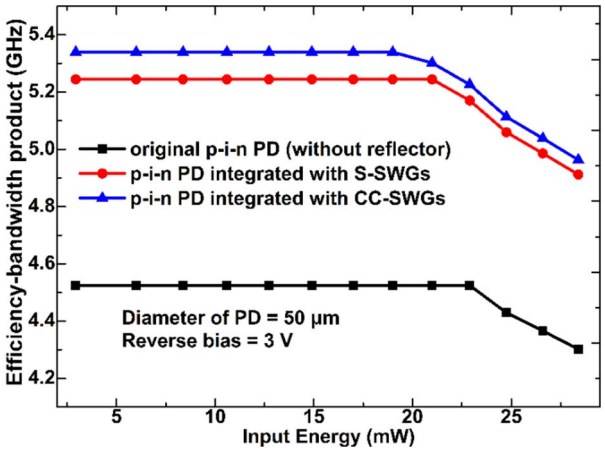

Fig. 7. Relationship between the efficiency-bandwidth product and the input power for different devices.

the efficiency-bandwidth product of the grating-integrated PD is much larger than that of the original PD, an improvement of 26%. The efficiency-bandwidth product of the grating-integrated PDs is first saturated with the increase of the incident optical power due to its increased responsivity. In addition, the efficiency-bandwidth product of the devices remains the same and then decreases as the input power increases due to the space charge effect. It is worth noting that the test process is carried out at room temperature without any cooling technique.

In conclusion, the p-i-n PDs, SOI-based nonperiodic S-SWGs, and nonperiodic CC-SWGs were fabricated, and then the PDs were integrated with the gratings. The experimental results show that the performance of the CC-SWGs was a little better than that of the S-SWGs. The p-i-n PDs integrated with either S-SWGs or CC-SWGs can simultaneously achieve a high responsivity and a high speed. For the grating-integrated PDs with a mesa diameter of 50 μm, the efficiency-bandwidth product increased by 26%, compared with the original PD. In addition, the responsivity of the grating-integrated PDs is enhanced in a wide spectral range compared with the original PD. The performance of the p-i-n PD with a small mesa diameter could be significantly improved by integration with the gratings especially when the FWHM of the grating focus was reduced to tens of microns by improving the fabrication process, according to our research findings.

The authors would like to thank Wenjing Fang for helpful discussions and data exchange. This work was supported by the Joint Laboratory of Quantum Optoelectronics and the Theory of Bivergentum and Beijing International Scientific and Technological Cooperation Base of Information Optoelectronics and Nano-heterogeneous Structure.

This work was funded by the National Natural Science Foundation of China (NSFC) (Nos. 61574019, 61674020, and 61274044), the 111 Project (No. B07005), the Beijing Municipality Natural Science Foundation (No. 4132069), and the Program for Changjiang Scholars and Innovative Research Team in University through the Ministry of Education of China (No. IRT0609).

References

1. K. Kishino, M. S. Unlu, J.-I. Chyi, J. Reed, L. Arsenault, and H. Morkoc, IEEE J. Quantum Electron. **27**, 2025 (1991).
2. H.-H. Tung and C.-P. Lee, IEEE J. Quantum Electron. **33**, 753 (1997).
3. C. C. Barron, C. J. Mahon, B. J. Thibeault, G. Wang, W. Jiang, L. A. Goldren, and J. E. Bowers, Electron. Lett. **30**, 1796 (1994).
4. Y. M. El-Batawy, M. J. Deen, and N. R. Das, IEEE J. Lightwave Technol. **21**, 2031 (2003).
5. X. Duan, Y. Huang, Y. Shang, J. Wang, and X. Ren, Opt. Lett. **39**, 2447 (2014).
6. Q. Chen, Y. Huang, X. Zhang, X. Duan, J. Fei, X. Ma, T. Liu, G. Wu, K. Liu, and X. Ren, IEEE Photon. Technol. Lett. **29**, 1203 (2017).
7. X. Duan, Y. Huang, X. Ren, Y. Shang, X. Fan, and F. Hu, IEEE Photon. Technol. Lett. **24**, 863 (2012).
8. C.-L. Hoa, M.-C. Wua, W.-J. Hob, and J.-W. Liaw, Solid-State Electron. **43**, 961 (1999).
9. J. N. Munday and H. A. Atwater, Nano Lett. **11**, 2195 (2010).
10. Y. Zhou, M. C. Y. Huang, and C. J. Chang-Hasnain, IEEE Photon. Technol. Lett. **20**, 434 (2008).
11. I.-S. Chung, V. Iakovlev, A. Sirbu, A. Mereuta, A. Caliman, E. Kapon, and J. Mørk, IEEE J. Quantum Electron. **46**, 1245 (2010).
12. W. Fang, Y. Huang, X. Duan, K. Liu, J. Fei, and X. Ren, Chin. Phys. B **25**, 114213 (2016).
13. W. Fang, Y. Huang, X. Duan, K. Liu, X. Ren, and J. Wang, in *Opto-Electronics and Communications Conference (OECC) and 2016 International Conference on Photonics in Switching (PS)*, Niigata, Japan, July 3-7, (2016), p. 1.
14. X. Duan, G. Zhou, Y. Huang, Y. Shang, and X. Ren, Opt. Express **23**, 2639 (2015).
15. D. Fattal, J. Li, Z. Peng, M. Fiorentino, and R. G. Beausoleil, Nat. Photon. **4**, 466 (2010).
16. Y. Yuan and J. Chen, Chin. Opt. Lett. **14**, 011404 (2016).
17. B. Gao, T. Chen, V. Khuat, J. Si, and X. Hou, Chin. Opt. Lett. **14**, 021407 (2016).
18. X. Duan, Y. Huang, H. Huang, X. Ren, Q. Wang, Y. Shang, X. Ye, and S. Cai, Opt. Express **18**, 5879 (2010).